J3.5 ACCOUNTING FOR PARTIALLY CLOUD-FILLED PIXELS USING MULTI-RESOLUTION IMAGER DATA

Louis, Nguyen, Patrick Minnis, David F. Young, William L. Smith, Jr.
NASA Langley Research Center, Hampton, VA 23681

Patrick W. Heck, Anita Rapp
AS&M, Inc., Hampton, VA

Sunny Sun-Mack
SAIC, Hampton, VA

1. INTRODUCTION

Partially cloud-filled pixels can be a significant problem for remote sensing of cloud properties. For example, optical depths and effective particle sizes are often too small or too large, respectively, when derived from radiances that are assumed to be overcast but contain radiation from both clear and cloud areas within the satellite imager field of view. Few methods have been developed for taking these effects into account, yet the results from such retrievals can bias the statistics of cloud properties making it difficult to match observations with model calculations of cloud parameters. One possible means for reducing the impact of such partially cloud filled pixels is to estimate the cloud fraction within each pixel. Although the nominal resolution for most channels on the Geostationary Operational Environmental Satellite (GOES) imager and the Moderate Resolution Imaging Spectroradiometer (MODIS) on Terra are 4 and 1 km, respectively, both instruments also take visible (VIS, 0.65 µm) channel data at 1 km and 0.25 km, respectively. Thus, it may be possible to obtain an improved estimate of cloud fraction within the lower resolution pixels by using the information contained in the higher resolution VIS data. The GOES and MODIS multi-spectral (0.64, 3.7, 11, and 12 µm) data are analyzed with the algorithm used for the Atmospheric Radiation Measurement Program and the Clouds and Earth's Radiant Energy System to derive cloud amount, temperature, height, phase, effective particle size, optical depth, and water path. Normally, the algorithm assumes that each pixel is either entirely clear or cloudy. In this study, a threshold method is applied to the higher resolution VIS data to estimate the partial cloud fraction within each low-resolution pixel. The cloud properties are then derived from the observed low-resolution radiances using the cloud cover estimate to properly extract the radiances due only to the cloudy part of the scene. This approach is applied to both GOES and MODIS data to estimate the improvement in the retrievals for each resolution. This technique is most likely to yield improvements for low and midlevel layer clouds that have little thermal variability in cloud height.

*Corresponding author address: Louis Nguyen, MS 420, NASA Langley Research Center, Hampton, VA 23681.
email: l.nguyen@larc.nasa.gov.

2. METHODOLOGY AND DATA

Minnis et al. (2002) describe the Visible Infrared Solar-infrared Split-window Technique (VISST) that uses the visible (VIS; 0.65 µm), infrared (IR; 10.8 µm), solar infrared (SIR; 3.9 µm) and split-window infrared (12.0 µm) channel to derive cloud height; phase; optical depth; effective particle size, either ice crystal diameter D_e or droplet radius r_e; and either liquid water path LWP or ice water path IWP for each GOES-8 pixel determined to be cloudy. The cloud mask CM (Trepte et al. 1999) consists of a decision tree that compares the observed VIS, IR, and SIR radiances with a set of thresholds based on the a priori estimates of the clear VIS reflectance, the skin temperature, the surface emissivities, the vertical profile of temperature and water vapor, and the variation of these values within a 0.5° box. A consistent value of clear or cloudy, in all three channels, results in an immediate classification of the pixel as clear or cloudy. Otherwise, a series of additional tests, "C tests," are performed to classify the pixel. If it is cloudy, then the observed radiances are used in the VISST to derive the cloud properties.

The nominal 4-km VIS data are actually sampled 1-km VIS radiances. Thus, to use the 1-km pixels P_1, the 4 x 4 array of 1-km pixels that matches the 4-km pixels P4 must first be determined. This is accomplished by computing the average reflectance for a series of 4 x 4 arrays created by shifting the starting line or element of the array within the image. These pixels are then assigned to the nearest IR pixel and a set of the matched VIS and IR pixels are correlated. The shifts in starting line and element corresponding to the highest correlation are then used to create a new averaged 4-km VIS reflectance and an array of 16 1-km VIS reflectances that are linked to a particular set of IR line and element coordinates. The line and element shifts for the 1-km data vary by 1 or 2 positions from image to image.

This new data set is then analyzed with the cloud mask to determine which 4-km pixels are cloudy. If the CM(P_4) is cloudy, then the 1-km data are tested using a simple clear-sky VIS reflectance threshold (CST).

Figure 1 shows a histogram plot of the clear, cloudy, and partially cloud-filled pixels from an adjacent clear and cloudy 0.5° regions. The reflectance curve from the 1km pixels (dash lines with filled circles) shows that the apparent clear-sky value is greater than what is indicated in the 4km pixels (dash line with open circles). To account for the variation in the clear-sky values, CST is computed using

$$CST = R + (3\sigma * 1.20)/\cos(\theta_o), \quad (1)$$

where R is the calculated 4km clear-sky reflectance, σ is the standard deviation in R, and θ_o is the solar zenith angle. The value 1.20 is the scale factor for the 20% difference in the 4km and 1km σ. If the 1km reflectance exceeds the CST, then the pixel is cloudy. The ratio of the cloudy 1-km pixels to 16 constitutes the cloud fraction C_4 for P_4. The value of C_4 is then sent to VISST, which computes the top-of-atmosphere radiance for each cloud model and wavelength as

$$R(C_4) = (1 - C_4)R_{cs} + C_4\, R(\text{cloud model}), \quad (2)$$

where R_{cs} is the clear-sky radiance for the particular channel. These calculated model values are then compared with the observed radiances to retrieve the cloud properties.

In this initial study, the computed CST is used to test each P_1 over a 0.5° region centered on the ARM CART site. Half-hourly GOES-8 data taken between 1200 and 2345 UTC on 19 March 2000 are analyzed using the P_4 data alone and then the P_1 data. Examples of the matched 4 and 1-km images are shown in Figure 2. The clouds are situated at approximately 1.5 km above the surface and marked by gaps that are primarily oriented along the north-south direction and by some smaller scale cellular structure evident in Fig. 2a.

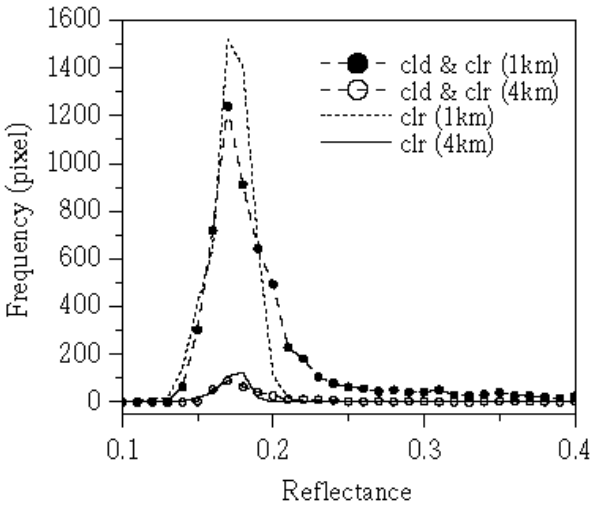

Fig 1. Histogram of both clear and partially cloud-filled 0.5° regions from GOES-8 visible image taken on March 19, 2000 at 17:45 UTC.

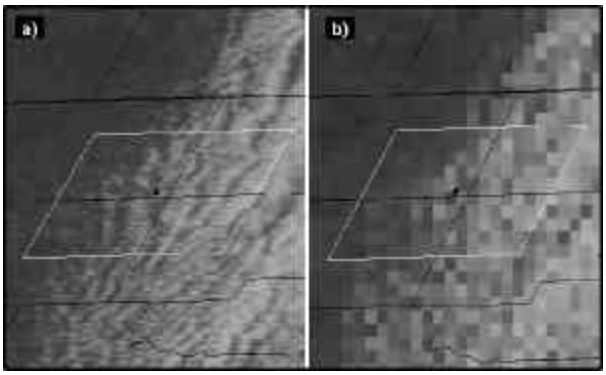

Fig 2. GOES-8 1km (a) and 4km (b) visible image taken at 17:45 UTC on 19 March 2000 showing 0.5° analysis region centered at the ARM Cart Site.

The cloud deck was moving from west to east during the day with the structure passing over the ARM CART site after 1700 UTC. Otherwise the clouds were unbroken. Figure 3 shows a comparison of the cloud fractions derived from the surface using CM(P_4), the whole-sky imager WSI, the ARM Active Remote Sensing Cloud Layer (ARSCL) product (Clothiaux et al. 2000), and the ARM Shortwave (SW) Flux Analysis Value Added Product (Gaustad and Long, 2002). During overcast conditions (1400 to 1700 UTC), CM(P_4) agrees well with the ARSCL and SW results. The CM(P_4) tracks fairly closely with the WSI and ARSCL during broken cloud conditions, except between 1900 and 2000 UTC, where CM(P_4) yields less cloud coverage than either instrument.

3. RESULTS

Figure 4 & 5 shows an example of the values of r_e

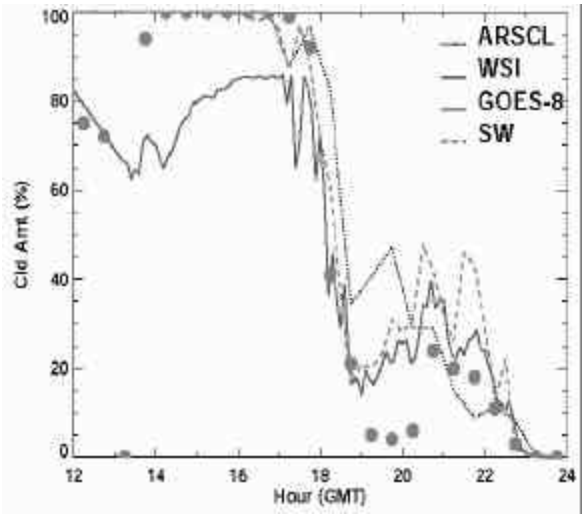

Fig 3. Time series of surface-based and GOES-8 cloud amounts, 19 March 2000.

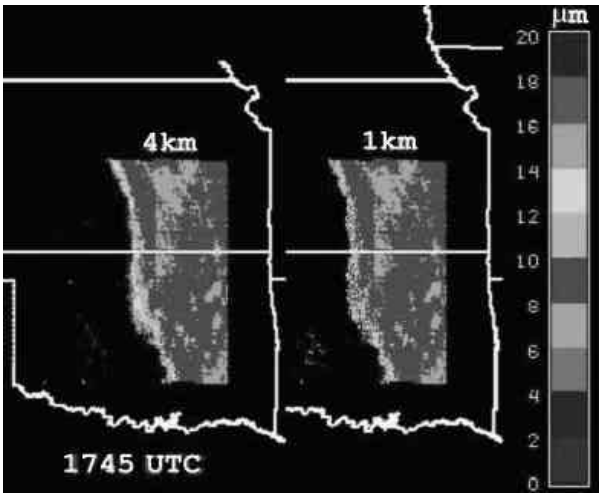

Fig 4. Cloud effective droplet radius from VISST, 19 March 2000.

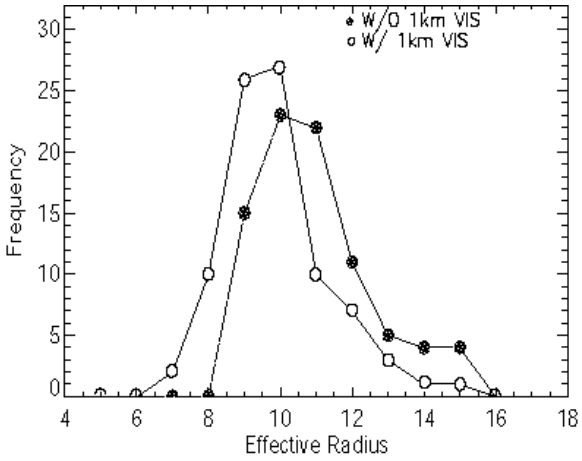

Fig 5. Cloud effective droplet radius from VISST using 0.5° region centered at the ARM Cart Site, 19 March 2000 17:45 UTC.

derived for the P_4 and P_1 datasets at 1745 UTC on 19 March 2000. Along the western edge of the cloud deck, r_e increases westward from about 10 μm to over 18 μm at 1745 UTC. By computing the cloud fraction for each pixel using 1km data, the peak of r_e shifts from 10-12 μm to 8-10 μm, and r_e rarely exceeds 12 μm in the same strip along the edge of the cloud deck, except for the southern fourth of area where little change is evident between the 4 and 1-km results. Apparently, in that area, the single-value threshold used for detecting clouds in the 1-km VIS data was too low and detected few 4-km pixels with $C_4 < 1$. The results for 1945 UTC are similar with few values exceeding 10 μm for the 1-km results. The droplet sizes for the scattered clouds west of the cloud deck decrease substantially when CM(P_1) is applied. The results in Fig. 4 are typical for the day.

The average P_1 and P_4 values of r_e for a 0.5° box centered on the ARM CART site are plotted in Fig. 6 with the results from Dong et al. (2002) that are based on surface radar and radiometer data. The mean effective radii from the satellite data diverge dramatically from the surface data beginning at 1600 UTC reaching values up 17 μm. The new P_1 results yield a maximum mean r_e of 12 μm, a value much closer to the peak derived from the surface data. Figure 7 demonstrates how the value of r_e decreased as a function of the original optical depth $t(P_4)$. The greatest changes occurred for the smaller optical depths indicating that the broken clouds along the edge of the deck were broken rather than optically thin.

4. DISCUSSION

This initial case clearly demonstrates that incorporation of higher resolution data, even when only one channel is available, yields more reasonable cloud properties than obtained with low resolution data only. However, much additional research is required before this type of approach can be implemented operationally. The assumption that a simple VIS threshold can discriminate between thin and broken clouds is valid only as long as the clouds in the larger pixel are thick enough to produce a significant VIS reflectance. Thin cirrus clouds are often nearly transparent at VIS wavelengths. Therefore, this approach should not be applied to cirrus clouds or the VIS threshold should be adjusted for the type of cloud in the pixel. One means for classifying each pixel as cirrus or otherwise would be to retain for each P_4 the classification of low, middle, or high cloud that is assigned each pixel in the layer bispectral threshold method (Minnis et al. 1995), the algorithm that serves as the initial step in the VISST.

One scenario for applying the 1-km enhancement method would be to select only low and midlevel clouds first. Then, a test for adjacent clouds could be used to determine those pixels that are on the edge of a cloud field. In the case of edge pixels, it may be possible to apply the technique to cirrus clouds to prevent an overestimate of D_e or an underestimate of t. Other approaches for implementing this method are certainly possible.

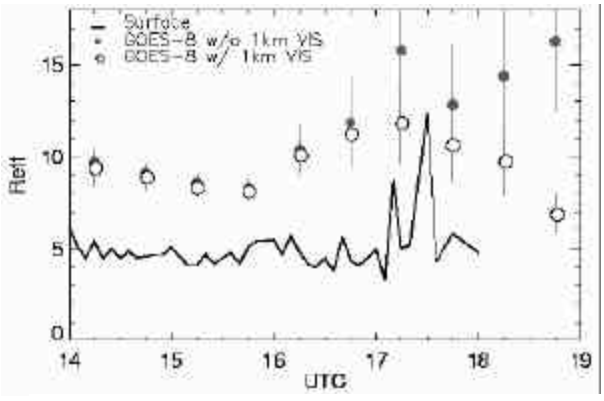

Fig 6. Comparison of cloud properties from the surface and 4 and 1km data, 19 March 2000.

It is clear from Fig. 1 that the local clear-sky reflectance and, hence, the 1-km VIS threshold should be characterized more accurately. Otherwise, large errors in the cloud fraction may result with subsequent errors in the derived properties. In this study, the cloud fraction was only computed for P_4's that had been classified as cloudy. However, there are probably pixels that are classified as dear that contain small amounts of clouds. Therefore, the criteria for computing sub-pixel fractional cloudiness should be expanded such that many of these smaller cloud amounts can be taken into account.

5. CONCLUSIONS AND FUTURE RESEARCH

The use of multi-resolution data for alleviating some of the errors in cloud property retrievals appears to be promising, at least for low and midlevel clouds. The approach does not account for the three-dimensional structure of the clouds and its effect on the radiances, which are assumed to come from plane-parallel clouds. That effect is likely to increase as the subpixel cloud fraction decreases. The method used here requires careful alignment of the 4 and 1-km pixels, a task that can be CPU intensive because the alignment appears to change slightly with each image.

This method is currently being applied to the Moderate Resolution Imaging Spectroradiometer (MODIS) on the Terra satellite. The initial results look promising but more work is required. Its application will require higher resolution maps of clear-sky reflectance than are currently used. Using such maps necessitates very accurate navigation of each imager pixel. The proper VIS thresholds for accurately detecting the subpixel clouds must also be established. The process will probably require thresholds that depend on the solar zenith angle and the background reflectance.

Finally, it should be noted that only one cloud case was examined here, so it is essential that many different cloud conditions should be tested with this approach before it can be implemented in any operational scheme. Such testing will use both multi-resolution data like GOES and MODIS, but will also involve the creation of artificial 4-km pixels from 1-km pixels that have radiances at all wavelengths.

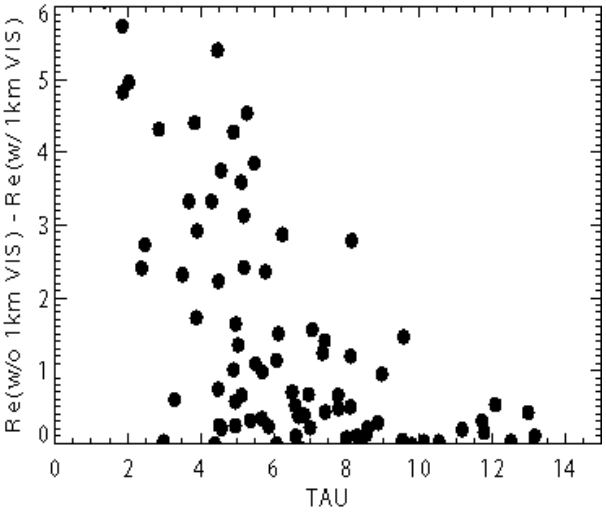

Fig 7. Decrease in r_e as a function of $t(P_4)$.

REFERENCES

Clothiaux, E. E., T. P. Ackerman, G. G. Mace, K. P. Moran, R. T. Marchand, M. Miller, and B. E. Martner, 2000: Objective determination of cloud heights and radar reflectivities using a combination of active remote sensors at the ARM CART sites. *J. Appl. Meteorol.*, **39**, 645-665.

Dong, X., P. Minnis, G. G. Mace, W. L. Smith Jr, M. Poellot, and R. Marchand, 2002: Comparison of stratus cloud properties deduced from surface, GOES, and aircraft data during the March 2000 ARM Cloud IOP. Accepted *J. Atmos. Sci.*

Gaustad, K.L. and C.N. Long, 2002: An Evaluation of Cloud Cover, Cloud Effect, and Surface Radiation Budgets at the SGP and TWP ARM Sites. *Proceedings of the Twelfth ARM Science Team Meeting,* St. Petersburg, FL, April 8-12, 20002.

Minnis, P., D. P. Garber, D. F. Young, R. F. Arduini and Y. Takano, 1998: Parameterizations of reflectance and effective emittance for satellite remote sensing of cloud properties. *J. Atmos. Sci.*, **55**, 3313–3339.

Minnis, P. et al., 1995: Cloud Optical Property Retrieval (Subsystem 4.3). In *Clouds and the Earth's Radiant Energy System (CERES) Algorithm Theoretical Basis Document, Volume III: Cloud Analyses and Radiance Inversions (Subsystem 4)*, *NASA RP 1376 Vol. 3*, edited by CERES Science Team, pp. 135-176.

Minnis, P., W. L. Smith, Jr., and D. F. Young, 2001: Cloud macro- and microphysical properties derived from GOES over the ARM SGP domain. *Proceedings of the ARM 11th Science Team Meeting*, Atlanta, GA, March 19-23, 11 pp. (available at http://www.arm.gov/docs/ documents/technical/conf_0103/minnis-p.pdf).

Trepte, Q., Y. Chen, S. Sun-Mack, P. Minnis, D. F. Young, B. A. Baum, and P. W. Heck, 1999: Scene identification for the CERES cloud analysis subsystem. *Proc. AMS 10th Conf. Atmos. Rad.*, Madison, WI, June 28 – July 2, 1999, 169-172.